Journal of Materials Chemistry C

RSC Publishing

PAPER

View Article Online
View Journal | View Issue

Cite this: *J. Mater. Chem. C*, 2013, **1**, 7009

Enhanced performance in polymer light emitting diodes using an indium–zinc–tin oxide transparent anode by the controlling of oxygen partial pressure at room temperature†

Soo Won Heo,‡[a] Yoon Duk Ko,‡[b] Young Sung Kim*[c] and Doo Kyung Moon*[a]

Received 26th April 2013
Accepted 10th August 2013

DOI: 10.1039/c3tc30789a

www.rsc.org/MaterialsC

The amount of indium in indium zinc tin oxide (IZTO) was reduced by over 20% by manufacturing an IZTO target containing ZnO for application as the transparent conducting oxide (TCO) anode of polymer light emitting diodes (PLEDs). The IZTO target was manufactured with the composition In_2O_3 (70 at%)–ZnO (15 at%)–SnO_2 (15 at%), and IZTO films were formed at room temperature using a pulsed DC magnetron sputtering system at oxygen partial pressures of 0–4%. The optical and electrical properties of the IZTO films and the device performance of PLEDs with IZTO film were characterized. Amorphous IZTO films prepared at an oxygen partial pressure of 3% showed the best properties. The resistivity, mobility, transmittance, figure of merit and work function of the IZTO film were 5.6×10^{-4} Ω cm, 44.59 $cm^2\ V\ s^{-1}$, 81% (visible region), 3.0×10^{-3} ohm^{-1}, and 5.56 eV, respectively. The PLEDs with the IZTO film deposited under the optimum conditions showed the maximum brightness and the maximum luminance efficiency of 23 485 cd cm^{-2} and 2.29 cd A^{-1}, respectively, which showed a 21% enhancement in device performance compared to PLEDs with commercial ITO film. In addition, the stability of the fabricated device was improved.

1 Introduction

The electrode properties of transparent conducting oxide (TCO) films in opto-electronic systems require >80% transmittance in the visible region (wavelength of 380–780 nm) and $<10^{-3}$ Ω cm conductivity.[1–9] TCOs can be applied to liquid crystal displays (LCDs), plasma display panels (PDPs), organic light emitting diodes (OLEDs), touch screen panels (TSPs), dye sensitized solar cells (DSSCs) and organic photovoltaic cells (OPVs). In general, TCOs, which consist of n-type semiconductor[10] and p-type semiconductor[11] materials, have attracted considerable attention. Indium tin oxide (ITO) is the most popular TCO owing to its low resistivity and high transparence in the visible light region.[12–14]

Nevertheless, there are critical problems in ITO transparent electrodes because of its properties and cost. ITO transparent electrodes generate cracks and fractures at low strains of 2–3% as a ceramic material.[15] In addition, salt, acid or device adhesives which exist naturally cause corrosion in the ITO layer, resulting in a decrease in its lifetime.[16,17] The high cost of indium is one of the largest problems in applying ITO as the TCO electrode of opto-electronic devices. ITO consists of a ratio of indium(III) oxide (In_2O_3) and tin(IV) oxide (SnO_2), with the optimal electro-optic properties occurring at a 90 : 10 weight ratio. Therefore, indium composes nearly 75% of the mass of a typical ITO film, and ITO is responsible for about $^3/_4$ of the global indium consumption.[18] Indium is a rare metal with limited reserves and is most commonly obtained as a by-product of zinc mining.[19] In addition, indium is very inefficient because only 3–30% of the ITO target is used to form ITO film in the sputter deposition process.[18,20] ITO electrode films in devices need to have a high deposition temperature (>300 °C) and are difficult to apply in flexible devices due to the low glass transition temperature (T_g) of plastic substrates.[9]

Therefore, it is important to develop technologies to reduce the amount of indium in ITO transparent electrodes, or produce indium-free transparent electrodes.[10,21–23] Furthermore, it is necessary to develop a high quality TCO electrode as an anode layer with a low processing temperature, low resistance, high transparency, smooth surface and high work function, since

[a]*Department of Materials Chemistry and Engineering, Konkuk University, 1 Hwayang-dong, Gwangjin-gu, Seoul, Republic of Korea. E-mail: dkmoon@konkuk.ac.kr; Fax: +82-2-444-0765*

[b]*U-PJT, Samsung display, #181, Samsung-ro, Tangjeong-Myeon, Asan-City, Chungcheongnam-Do, Republic of Korea*

[c]*Graduate School of NID Fusing Technology, Seoul National University of Science & Technology, 138 Gongneung gil, Nowon-gu, Seoul, Republic of Korea. E-mail: youngsk@snut.ac.kr; Fax: +82-2-970-6011*

† Electronic supplementary information (ESI) available. See DOI: 10.1039/c3tc30789a

‡ These authors contributed equally to this work.

OLEDs or PLEDs have drawn much interest as next generation displays.[24] Recently, multi-component and combinations of binary or ternary oxide systems have been assessed as replacements for ITO.[22] Materials researched include fluorine, gallium, aluminum, zinc, *etc.*, and transparent electrodes of fluorine-doped tin oxide (FTO),[25] gallium-doped zinc oxide (GZO)[26] and aluminum-doped zinc oxide (AZO)[27] have been reported. Among these oxide systems, indium zinc tin oxide (IZTO), which reduces the amount of indium and contains ZnO, is considered a potential material to replace ITO.[28–30] In addition, IZTO has a high work function, low resistivity, low sheet resistance and high transmittance despite the low deposition temperature. Therefore, it can be applied to plastic substrates and has the advantage of manufacturing flexible display electrodes. Bae *et al.* reported that an IZTO anode film can be an alternative material for highly efficient phosphorescent OLEDs.[31] Heo *et al.* demonstrated that amorphous IZTO films, which have good mechanical durability, could be used as an anode in flexible OLED devices.[32] In a previous study, we reported the transparent conducting properties and mechanical durability of amorphous IZTO films grown on a flexible polyimide substrate.[33]

TCOs applied to opto-electronic devices are generally manufactured by magnetron sputtering. TCO thin films are sensitive to the deposition power, gas pressure, temperature and oxygen flow rates of the sputtering system, and the optimization of the deposition conditions is essential for anodes in organic-based devices. In particular, among the sputtering deposition process conditions of TCO electrode films, the oxygen partial pressure $[O_2/(O_2 + Ar)]$ affects the electrical resistivity and optical transmittance. Despite this, there have been no specific studies of the effect of oxygen on the electrical, optical and structural properties of IZTO films deposited under a range of oxygen partial pressures.

Therefore, in this study, the IZTO target and IZTO TCO electrode film were manufactured with a composition of In_2O_3 (70 at%)–ZnO (15 at%)–SnO_2 (15 at%). The IZTO films were manufactured at room temperature under a range of oxygen partial pressures by pulsed DC magnetron sputtering. The interrelations between the chemical binding state and work function of the surface and the characteristics of the IZTO films were analyzed by X-ray photoelectron spectroscopy (XPS) and ultraviolet photoemission spectroscopy (UPS). In addition, the PLEDs with the IZTO transparent anode were fabricated and the performance of the fabricated devices were characterized.

2 Experiment

2.1 Deposition and characterization of IZTO films on a glass substrate

The IZTO films were deposited on glass (Corning product 1737 Eagle 2000 glass) under various oxygen partial pressures by pulsed DC magnetron sputtering. The target (In_2O_3 (70 at%)–ZnO (15 at%)–SnO_2 (15 at%)) was prepared by mixing and sintering powders. The glass substrate was cleaned in an ultra-sonicator successively with acetone, isopropyl alcohol and de-ionized water. The substrates were dried by blowing N_2 gas, and loaded into the sputtering chamber. The sputter deposition was carried out at room temperature with a working pressure of 6 mTorr. The input power and frequency were 125 W and 30 kHz, respectively. The flow ratio of O_2 was altered from 0.0–4.0% $[O_2/(O_2 + Ar)]$ and the thickness of the IZTO films was 200 nm.

The crystal structures of the films were analyzed by X-ray diffraction patterns (XRD; D8 ADVANCE, Bruker, Germany), and the crystal phase was reviewed with samples processed by focused ion beam (FIB; NOVA600 NanoLab, FEI, Holland) through STEM (JEM-2100(HR) + Cs corrector, JEOL/CEOS, Japan). The surface morphology was analyzed by atomic force microscopy (AFM; XE-100, PISA, Korea) and field emission scanning electron microscopy (FESEM; S-4800, HITACHI, Japan). The composition of the IZTO films was estimated using field emission SEM/EDS(S-4800, HITACHI/7593-H, HORIBA) and the results are reported in Table S1, ESI.† The electrical properties, including the resistivity, carrier concentration and mobility of the IZTO films, were measured using the van der Pauw method with the Hall measurement system (HMS-3000, ECOPIA, Korea). The transmittance of the films was measured using a UV-visible spectrometer (S-3100, SCINCO, Korea). X-ray photoelectron spectroscopy (XPS; ESCA 2000, VG Microtech, UK) was used to confirm the surface chemical state, and the work functions of the thin films were measured by ultraviolet photoemission spectroscopy (UPS; AXIS-NOVA, Kratos Inc., England).

2.2 Fabrication and characterization of PLEDs with the IZTO transparent anode

To clean the glass coated with IZTO, sonication was performed for 5 minutes successively with detergent (Alconox© in deionized water, 10 wt%), acetone, isopropyl alcohol (IPA) and deionized water. Moisture was removed by blowing N_2 gas and the substrate was completely dried for 10 minutes by annealing in a 110 °C hot plate. The IZTO glass was cleaned for 10 min with an ultra-violet ozone (UVO) cleaner. The yellow emitting polymer (Super yellow, Merck, Germany) for the emitting layers was dissolved (0.5 wt%) in chlorobenzene, shaken for 24 h and filtered through a 5 um PTFE syringe filter. The yellow polymer was coated with an 80 nm thickness, and the residual solvents were removed by annealing for 1 h at 90 °C. The metal electrode was deposited thermally in a high vacuum chamber ($<1 \times 10^{-6}$ torr) in the order of BaF_2 (0.1 Å s^{-1}, 2 nm), Ba (0.2 Å s^{-1}, 2 nm) and Al (5 Å s^{-1}, 200 nm). Getters were attached inside the glass cover and encapsulated to protect the organic layers and the cathode from H_2O and O_2. The electrical and optical properties of the PLEDs were characterized using a Keithley 2400 source meter unit (Keithley, USA) and PR 670 spectra scan (Photo Research, USA).

3 Results and discussion

Fig. 1 shows the XRD patterns of the IZTO film deposited by pulsed DC magnetron sputtering. The plasma power and working pressure were 125 W and 6 mTorr, respectively. The films were deposited at room temperature by changing the

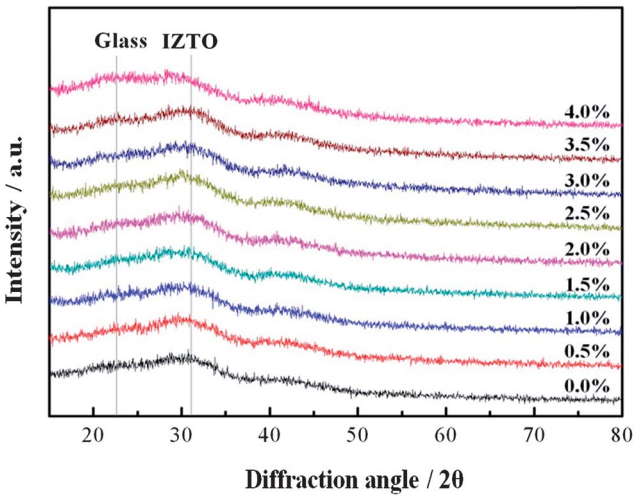

Fig. 1 X-ray diffraction patterns of the IZTO films with various oxygen partial pressures on the glass substrate.

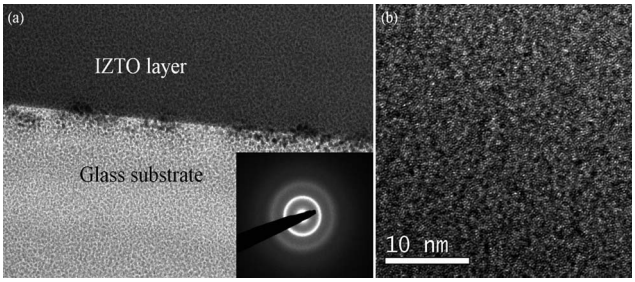

Fig. 2 (a) Cross-sectional HRTEM image of the IZTO film (inset: SAED pattern), and (b) bright-field image obtained from an IZTO film (3.0% oxygen partial pressure) grown on a glass substrate.

oxygen partial pressure at 0.5% intervals between 0.0 and 4.0%. The IZTO films showed a broad peak at the glass substrate ($2\theta = 23^\circ$) and the IZTO layer ($2\theta = 31^\circ$) regardless of the oxygen partial pressure. The sputtering process is performed at room temperature and all of the IZTO films showed an amorphous structure. Generally, the In_2O_3 (ITO) films deposited with SnO_2 have a low amorphous–crystalline transition temperature, causing rapid crystallization even at low substrate temperatures (~150 °C). On the other hand, the In_2O_3 (IZO) films doped with ZnO have a higher amorphous–crystalline temperature than the case above and maintain a stable amorphous structure up to 500 °C.[34] The IZTO films have a stable amorphous structure similar to the IZO film because of the immiscibility of SnO_2 and ZnO in In_2O_3. Generally, the ITO films were manufactured at room temperature, unintentional surface heating is generated by plasma irradiation in the sputtering system, leading to crystallization in the film, which shows an oriented crystalline structure.[35] Meanwhile, the IZTO film manufactured in the study is heated by being exposed to the plasma during the pulsed DC magnetron sputtering, but shows a stable amorphous structure due to the thermal stability of the IZTO film.

The internal micro-crystal structure of the IZTO film was manufactured on the glass substrate under electrically and optically optimized conditions using the high resolution transmission electron microscopy (HRTEM) method (3.0% oxygen partial pressure in the study). Fig. 2(a) shows a cross-section HRTEM image, with the selected area electron diffraction (SAED) pattern in the inset, of the IZTO film. The uniform contrast of the IZTO layer shows that the IZTO film deposited on the glass substrate has an amorphous structure. The SAED pattern (Fig. 2(a), inset) of the IZTO film shows a diffused ring pattern with amorphous structures. Fig. 2(b) shows a bright-field image of the IZTO film. A few clusters, <10 nm in diameter, were observed from the diffraction contrast but there appears to be an amorphous structure with no distinctive features, which coincides with the results from the prior XRD tests.

The surface morphology of the IZTO films and the ITO (reference) film manufactured on the glass substrate with variable oxygen partial pressures was observed by FESEM, and the results are plotted in Fig. 3. The ITO film has a crystallized structure with a preferred orientation and a relatively rough surface, as shown in Fig. 3(f).[36] On the other hand, the IZTO films manufactured at room temperature have no defects, such as pinholes, cracks and protrusions, as shown in Fig. 3(a)–(e), owing to their stable amorphous structure with very fine particle shapes and a very smooth structure.

Fig. 4 shows the surface roughness of the deposited IZTO films under various oxygen partial pressures and of ITO film, determined by AFM. The surface roughness of the films was quantified by the root mean square (RMS) value. The RMS values increased with the increasing oxygen partial pressure, but all of the IZTO films had a relative smooth surface with a RMS roughness <0.5 nm (ITO RMS roughness: 1.845 nm, Fig. 4(f)). The IZTO films have low RMS values due to the non-crystalline structure with high thermal stability, and the low preparation temperature of the IZTO materials. TCO films with a low RMS roughness are important for the high performance of PLEDs because the surface roughness of the TCO anode films is closely related to the leakage current or current concentration in the PLEDs with the current driving method.[37] Therefore, the IZTO films manufactured in this study have a uniform surface roughness with an amorphous structure, and they are expected to have more stable and effective performance for device applications including flexible displays or PLEDs than ITO films.

The resistivity, mobility and carrier concentration of the IZTO films were measured using a Hall measurement system, and the results are plotted in Fig. 5. The results show that the electrical properties of the IZTO films in the sputtering process are quite sensitive to the oxygen partial pressure. The resistivity of the IZTO films decreased with increasing the oxygen partial pressure from 0.0 to 3.0%. On the other hand, the resistivity of the IZTO films increased with further increases in oxygen partial pressure beyond 3.5%. As a result, the lowest resistivity of the IZTO films was achieved by the oxygen partial pressure of 3.0%. To understand this trend, it is important to consider the source of the electrical charge carriers in thin films. The electrical charge generation in amorphous IZTO films consists of the following two issues described below.

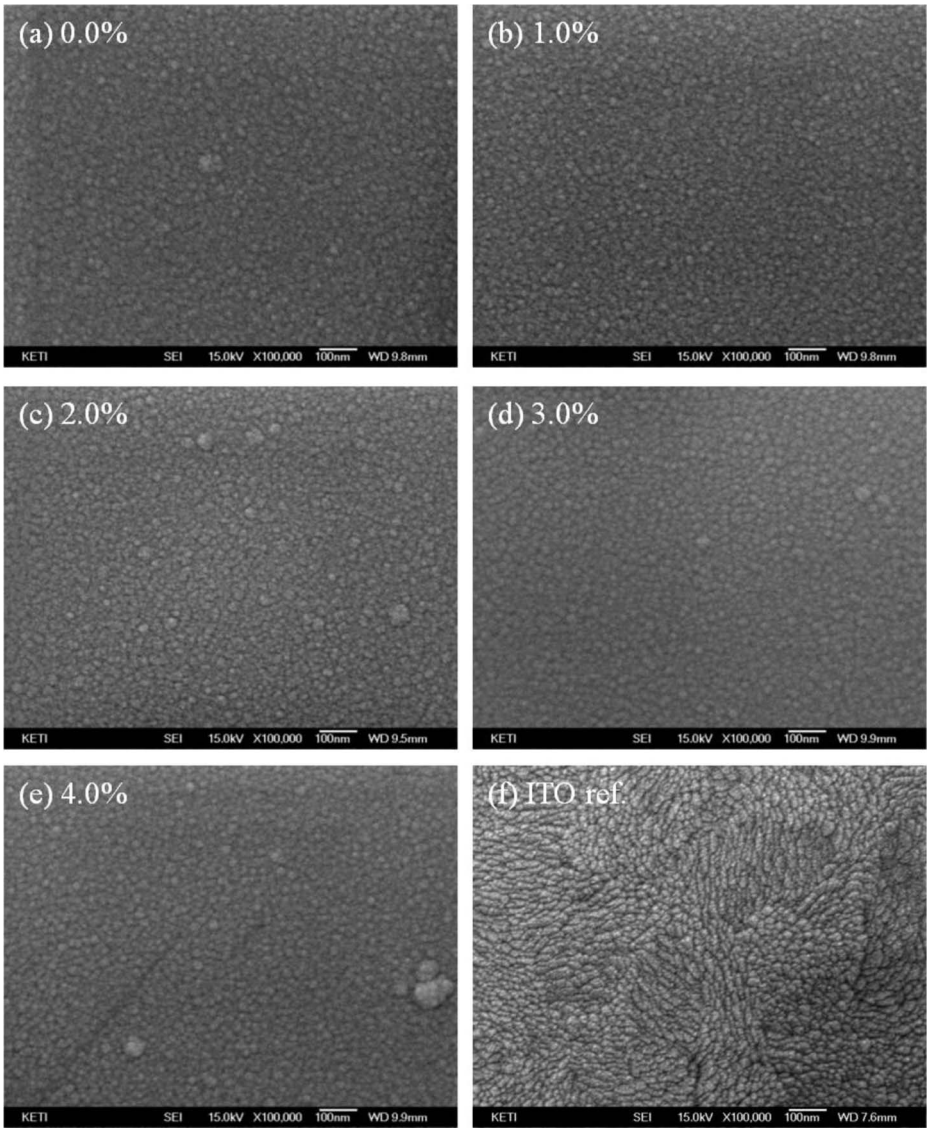

Fig. 3 FESEM images of the IZTO films with various oxygen partial pressures: (a) 0.0%, (b) 1.0%, (c) 2.0%, (d) 3.0% and (e) 4.0%, and (f) reference ITO.

Firstly, the replaced Sn^{4+} at the In^{3+} site in the locally ordered region of the amorphous matrix is considered to be an effective dopant, and may contribute to the electrical charge carriers in the degenerated n-type semiconductors despite the amorphous nature of the IZTO films.[28] In addition, the high deficiency of oxygen generated by unintentionally doped Zn and Sn generates doubly charged oxygen vacancies which have the features of n-type semiconductors.[28] The doping concentrations of Zn and Sn were fixed in this study and only the oxygen partial pressure was changed to optimize the resistivity of the IZTO film. In_2O_3, ZnO and SnO_2 lose oxygen during the deposition on a glass substrate from the IZTO target, forming non-stoichiometric films. Nevertheless, use of the correct amount of the oxygen gas during sputtering contributes to the generation of carriers such as oxygen vacancies.[38] Many studies related to ITO or IZO have reported that the lowest resistivity may be achieved by adding a small amount of oxygen gas.[39] The IZTO film manufactured with no injected oxygen gas shows an extremely high resistivity ($\sim 1.5 \times 10^4$ Ω cm) due to the low carrier concentration and mobility. Such a high resistivity increases scattering; the scatter centers exist as oxide complexes and the inefficient activation of Sn in the amorphous structure does not contribute to the carriers.[40] As the oxygen partial pressure is increased from 0.0 to 1.0%, the carrier concentration and mobility increase, and the resistivity of the IZTO films decreases sharply. On the other hand, as the oxygen partial pressure exceeds 1.5%, the carrier concentration decreases because the incorporation of excess oxygen ions (O^{2-}) removes oxygen vacancies. As the scatter centers are removed by the decreasing number of electric charge carriers, however, a compensation effect occurs, which increases the carrier mobility. As a result, the deposited IZTO film with a 3.0% oxygen partial pressure shows the lowest resistivity of 5.6×10^{-4} Ω cm. The resistivity of the IZTO film manufactured at room temperature may be comparable to the resistivity of a conventional ITO film manufactured at high temperature.

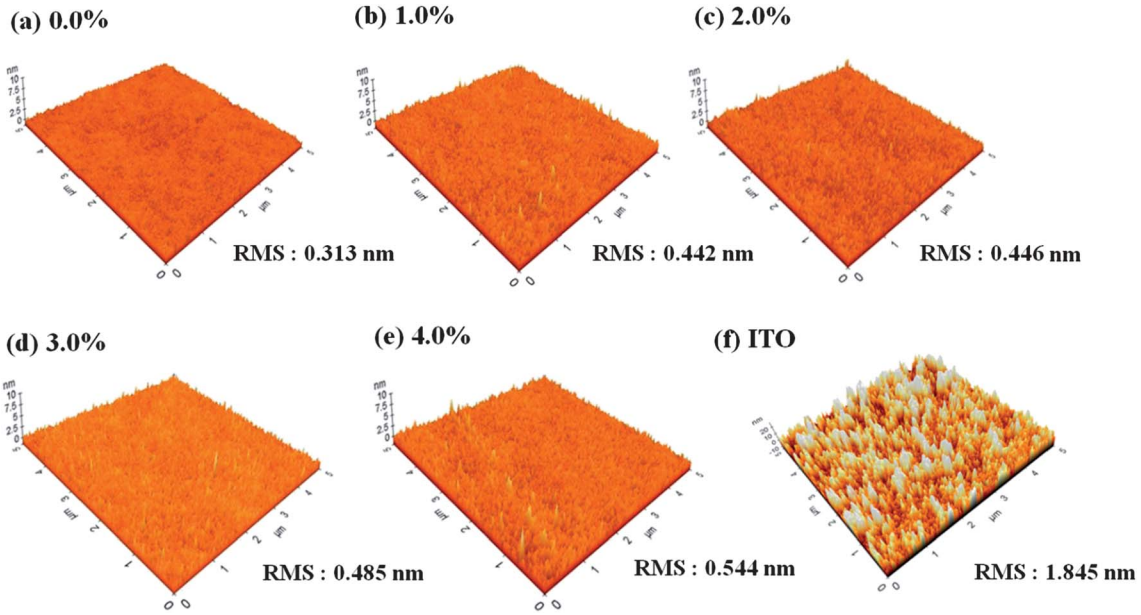

Fig. 4 AFM images and surface roughness of the IZTO films with various oxygen partial pressures: (a) 0.0%, (b) 1.0%, (c) 2.0%, (d) 3.0% and (e) 4.0%, and (f) reference ITO.

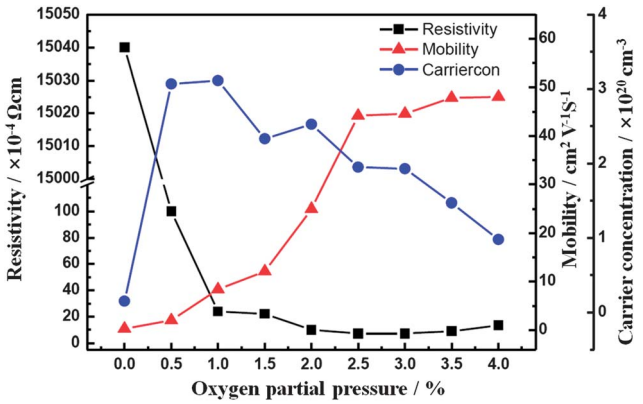

Fig. 5 Variations of the resistivity, mobility and carrier concentration of the IZTO films with different oxygen partial pressures.

In order to understand the conduction mechanisms in amorphous IZTO films, the sources of electrical charge carriers in the films should be considered. Yang *et al.* reported that, regardless of the crystallinity, the oxygen vacancies would be the prevailing contributor of the electrical charge carriers in IZTO films.[41] Lee *et al.* also reported that the substitution of Sn^{4+} ions in the In^{3+} sites was caused by some locally ordered regions in the amorphous matrix.[42] However, in the case of amorphous IZTO films, the Sn dopant is not sufficiently activated due to its low deposition temperature. In addition, only the oxygen content in the deposition atmosphere was varied in our system, so the variation of charge carriers in amorphous IZTO films can be determined by the oxygen vacancies. This is why the chemical binding state of oxygen is closely related to the carrier concentration. The available electronic charge concentration would decrease, but the increase in charge carrier mobility would compensate for this due to the removal of scatter centers. Therefore, the mobility of amorphous IZTO films increases with the decrease of the carrier concentration.

The optical transmittance of the IZTO films deposited under various oxygen partial pressures was measured using a UV-visible spectrometer, and the results are plotted in Fig. 6. The optical transmittance was <60% (at 550 nm) with a 0.0–1.5% oxygen partial pressure, but the optical transmittance increased at oxygen partial pressures >2.0%. In the sputtering process with In_2O_3, the ZnO and SnO_2 mixed oxide target, a metal like, dark film will be formed due to the loss of oxygen.[43] Therefore, the zero or low oxygen partial pressure may not be enough to compensate for the loss of oxygen during the sputtering process and results in a low transmittance. On the other hand, the input of a suitable oxygen flow can compensate for the loss of t oxygen during the sputtering process and result in a high optical transmittance. The results clearly show that adding a suitable amount of oxygen gas significantly improves the optical transmittance of the IZTO films. In particular, the IZTO films manufactured with oxygen partial pressures of 3.0–4.0% show >80% optical transmittance within the visible range (380–780 nm), which is similar to conventional ITO films which exhibit 85% transmittance.

Fig. 6(b) shows the absorption coefficient (α) as a function of the photon energy ($h\upsilon$) to examine the optical energy band gap of the IZTO films with variable oxygen partial pressures. The energy band gap of the films was determined by eqn (1):[44]

$$\alpha(h\upsilon) = D(h\upsilon - E_g)^{1/2} \quad (1)$$

where D is a constant for each material and E_g is the optical band gap.

An extrapolation of the straight line portion to the energy axis of the plot shows the optical energy band gap for each film, and the results are plotted in the inset of Fig. 6(b)

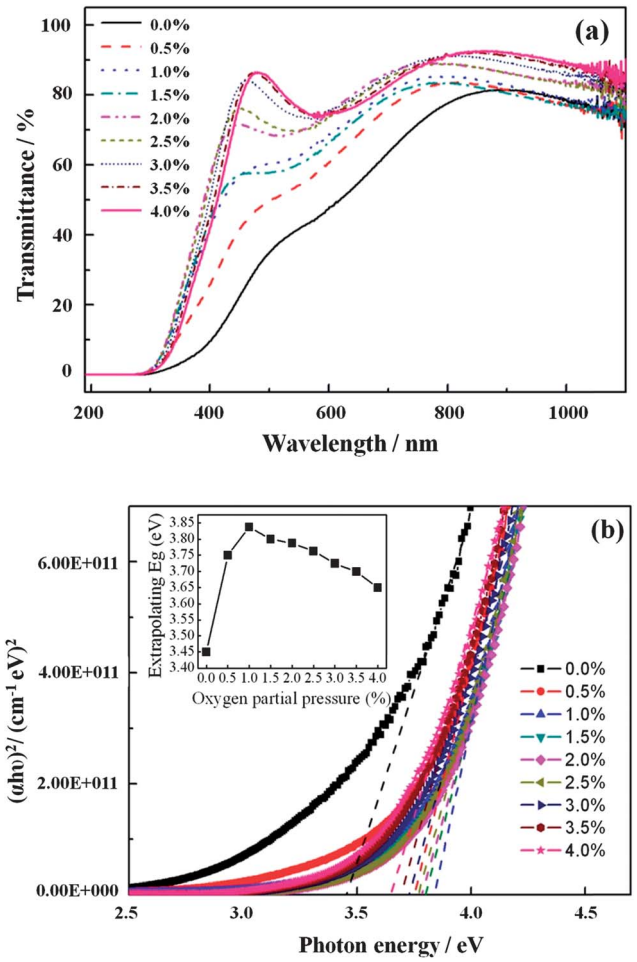

Fig. 6 (a) Optical transmission spectra of the IZTO films at various oxygen partial pressures, and (b) plot of $(\alpha h\nu)^2$ *vs.* photon energy for the IZTO films grown at various oxygen partial pressures, with the inset showing the band gap energies of the IZTO films.

The optical band gap of the IZTO films was quite sensitive to the oxygen partial pressure during the sputtering process, and the optical band gap decreased gradually with increasing oxygen partial pressure, and increases under the conditions where the electrically and optically improved oxygen partial pressure is >1.0%. The band structures of the IZTO films based on undoped In_2O_3 show parabolic conduction and valence bands. The optical band gap energy of the IZTO films, which are degenerate semiconductors, increases or decreases depending on the carrier concentration. The band gap widening (ΔE_g^{BM}) appears to be due to the increasing carrier concentration in the TCO film, which is called the Burstein–Moss (BM) effect.[45] The conduction band of the IZTO films is filled partially by electrons as Sn and Zn are doped into In_2O_3, and the corresponding Fermi level is located inside the conduction band. The Fermi level moves to a higher energy state in the conduction band with the increasing carrier concentration, and the BM effect appears to be due to band gap widening as the transition to a lower energy state is blocked. On the other hand, the decrease in the optical band gap inside the TCO films may be explained by band gap narrowing (ΔE_g^{N}) due to the electron-impurity scattering effect, impurity-induced potential fluctuation, and the merging of donor and conduction bands.[46,47] Therefore, band gap widening (ΔE_g^{BM}) and band gap narrowing (ΔE_g^{N}) are closely related to the change in carrier concentration in the IZTO film and can be expressed as eqn (2):

$$E_g = \Delta E_g^{BM} - \Delta E_g^{N}. \quad (2)$$

As mentioned in Fig. 5, the IZTO films manufactured in this study tend to display a decreased carrier concentration against the oxygen partial pressure increase, and the optical band gap also decreases with weak band gap widening (ΔE_g^{BM}).

Fig. 7 shows the XPS core level spectra of O 1s, In 3d, Zn 2p and Sn 3d. The chemical binding states of the IZTO films under various oxygen partial pressures were analyzed by XPS. There were no specific changes in the In 3d, Zn 2p and Sn 3p peaks despite the increasing oxygen partial pressure. On the other hand, as shown in Fig. 7(a), the higher binding energies of the O 1s peaks in the IZTO films decrease with the increasing oxygen partial pressure. Fan *et al.*[48] distinguishes the O 1s data as the O_I and O_{II} peaks of O^{2-} ions. The higher binding energy peak of O^{2-} (O_I) and the lower binding energy peak (O_{II}) coincide with the amount of oxygen vacancies and the six nearest-neighbor O^{2-} ions (O_I) with 531.6 eV, (O_{II}) with 529.9 eV which are neighbored with In atoms, respectively.[48] In our study, the binding energy ratios ($I(O_I)/I(O_{II})$) of the IZTO thin films with oxygen partial pressures of 0.0%, 1.0%, 2.0%, 3.0% and 4.0% were 1.95, 1.86, 1.63, 1.47 and 1.36, respectively. Therefore, it is concluded that the number of oxygen vacancies decreases on increasing the oxygen partial pressure from 0.0 to 4.0%. However, the film deposited at an oxygen partial pressure of 0% show a relatively low carrier concentration due to oxide complexes formed by excessive oxygen vacancies. The tendency of the O 1s peak intensity between 1.0 and 4.0% coincides with the results of the electrical carrier concentration shown in Fig. 5. Therefore, the electrical carrier concentration of IZTO thin films is closely related to the O 1s peak ratio ($I(O_I)/I(O_{II})$) observed by XPS.

The work functions of the IZTO film were observed to assess the alternative to the ITO film for transparent electrode applications. TCO films as the anode and low work function metals as the cathode are used as electrodes for organic (or polymer)-based light-emitting diodes, respectively. Therefore, the TCO electrode film with a high work function may decrease the hole injection barriers of the HOMO levels in the emitting layer materials and increase the efficiency of the PLEDs. The work functions of the IZTO films with variable oxygen partial pressures are measured by the inelastic secondary electron cutoff of the UPS energy distribution in an ultrahigh vacuum state (Fig. 8). Sugiyama *et al.* reported that the work function of doped In_2O_3 films is affected by surface contamination, oxygen status and the dopant concentration. In particular, an increase in the surface oxygen concentration may increase the work functions.[49] In the present study, the dopant concentration was fixed during the IZTO film deposition and the samples were prepared under the same cleansing conditions to measure the UPS. Therefore, the work functions of the IZTO films

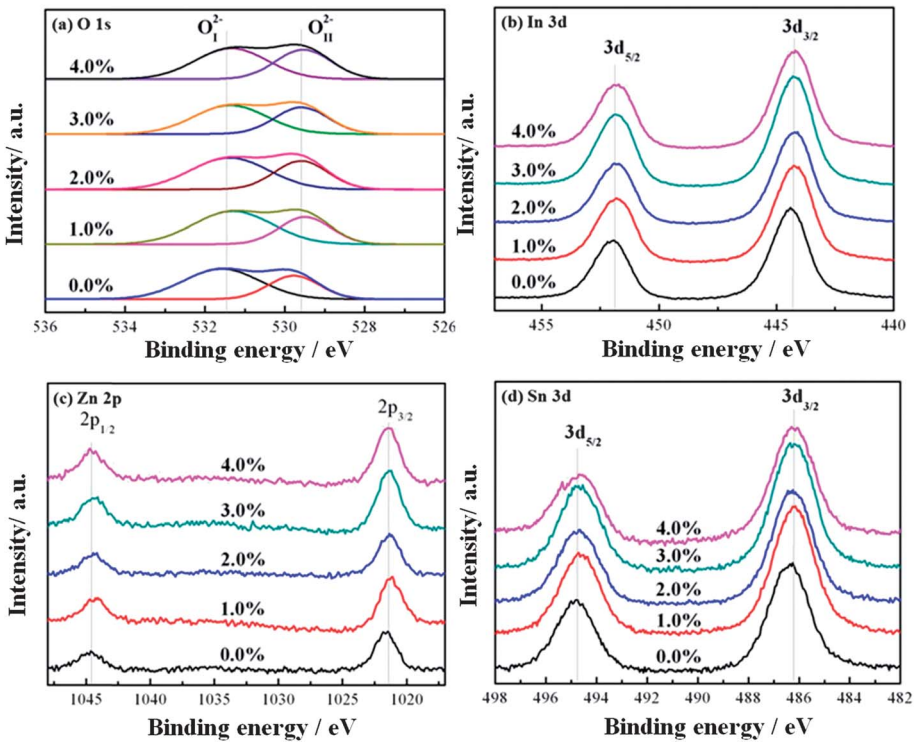

Fig. 7 XPS core level spectra of (a) O 1s, (b) In 3d, (c) Zn 2p and (d) Sn 3d obtained for the IZTO films grown on a glass substrate as a function of the oxygen partial pressure.

manufactured under various oxygen partial pressures are affected mainly by oxygen vacancies which form donor states. Therefore, the work functions increase due to the removal of oxygen vacancies in the electrically and optically stabilized IZTO films as the oxygen partial pressures increase. These results coincide with the electrical carrier concentration and XPS O 1s peak ratio changes. The work functions of the IZTO films manufactured under various oxygen partial pressures have high values (all over 5.4 eV) compared to the conventional ITO film (4.7 eV). Accordingly, the features of the newly fabricated PLEDs are improved due to the lower hole-injection barrier between the HOMO levels of the emitting layer materials and the increased work functions of the IZTO film.

Haacke proposed the figure of merit (Φ_{TC}) value as an effective tool for comparing the performance of TCO films with similar optical transmittances and resistivities.[50] Φ_{TC} can be

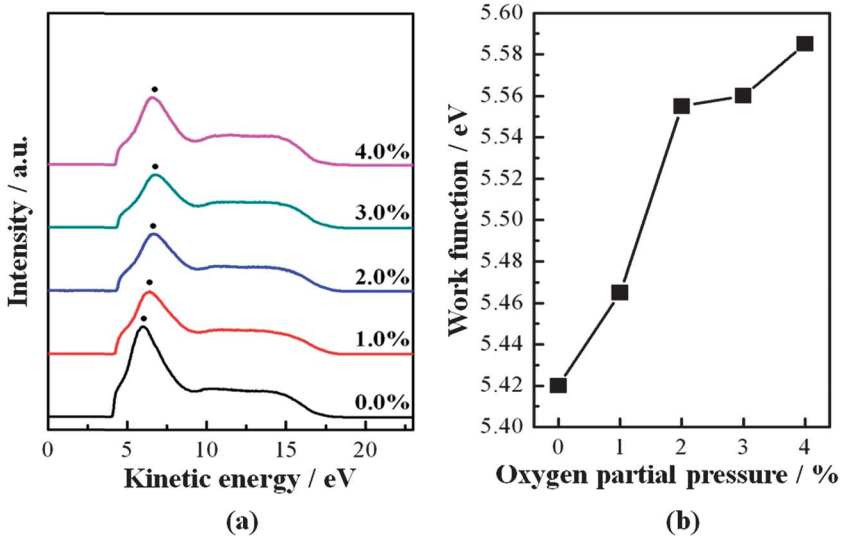

Fig. 8 (a) Low kinetic energy cutoffs of the IZTO films with UPS and the work function of the IZTO films deposited at various oxygen partial pressures.

calculated using eqn (3) from the results of the optical transmittance (T) and sheet resistance (R_{sh}) of the IZTO film under the variable oxygen partial pressures, as shown in Fig. 9.

$$\Phi_{TC} = T^{10}/R_{sh} \quad (3)$$

As expected from the results of the electrical and optical properties, the Φ_{TC} value of the IZTO films was highest at a 3.0% oxygen partial pressure. On the other hand, the Φ_{TC} value decreased with increasing electrical resistivity under 3.5–4.0% oxygen partial pressures. The electrical and optical properties can be optimized and improved by injecting a suitable amount of oxygen gas during the IZTO film deposition at room temperature.

PLEDs were fabricated and characterized to introduce the IZTO electrode film as a TCO for opto-electronic devices under oxygen partial pressures (IZTO (200 nm)/Yellow emitting polymer (80 nm)/BaF_2 (2 nm)/Ba (2 nm)/Al (200 nm)). Furthermore, the PLED using an ITO transparent anode was manufactured to compare the performance of the IZTO transparent anode. The reference ITO thin film deposited at 300 °C, manufactured by Samsung Precision Glass Co., showed a resistivity of 1.5×10^{-4} Ω cm and a transmittance higher than 85% (ITO (170 nm)/PEDOT : PSS (40 nm)/Yellow emitting polymer (80 nm)/BaF_2 (2 nm)/Ba (2 nm)/Al (200 nm)).

Fig. 10(a) and (b) show the brightness–voltage and luminance efficiency–current density characteristics of the PLEDs, respectively, and the results are presented in Table 1. The maximum brightness and the maximum luminance efficiency of the PLEDs manufactured with the IZTO film at an oxygen partial pressure of 3.0% were 23 485 cd m^{-2} and 2.29 cd A^{-1}, respectively. As shown in Table 1, the values of Φ_{TC} of the IZTO films deposited with oxygen partial pressures of 1.5–4.0% and the device performances coincide precisely. Therefore, the oxygen partial pressure was optimized at 3.0% as a result of the Φ_{TC} value and PLED performance.

The PLEDs with the ITO film were manufactured under the same conditions as the PLEDs with IZTO film to compare the device performance. The maximum brightness and the maximum luminance efficiency of the PLEDs with the ITO film were 23 228 cd m^{-2} and 1.88 cd A^{-1}, respectively. The maximum brightness of the PLEDs with the IZTO film was similar to that of the PLEDs with the ITO film. However, the maximum luminance efficiency of the PLEDs with the IZTO film was 2.29 cd A^{-1} and was improved by 21% compared to the device with the ITO film. The reason why the PLEDs with the IZTO film have a higher efficiency than the PLEDs with ITO film may be explained by the energy band diagram in Fig. 11. As shown in Fig. 11(a), the work function of the ITO film is 4.7 eV. It is difficult to inject the holes from the ITO film to the emitting layer. In order to effectively inject the holes from the ITO film to the emitting layer, therefore, PEDOT : PSS (5.2 eV) as a hole transporting layer is required. However, the IZTO film has a higher work function than that of the ITO/PEDOT : PSS structure. Therefore, the device features an ohmic contact without the PEDOT : PSS layer, and the holes can be easily injected into the emitting layer due to their low energy barrier. Therefore, PLEDs with IZTO films have a lower turn-on voltage (2.8 V, oxygen partial pressure at 3.0%) than PLEDs with ITO (3.2 V). It can be seen that the lower energy barrier attributed to the significant improvement of the device performance.

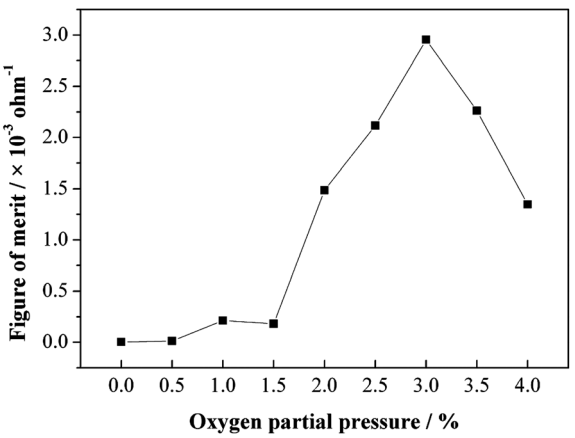

Fig. 9 Calculated figure of merit value for the IZTO films grown at various oxygen partial pressures.

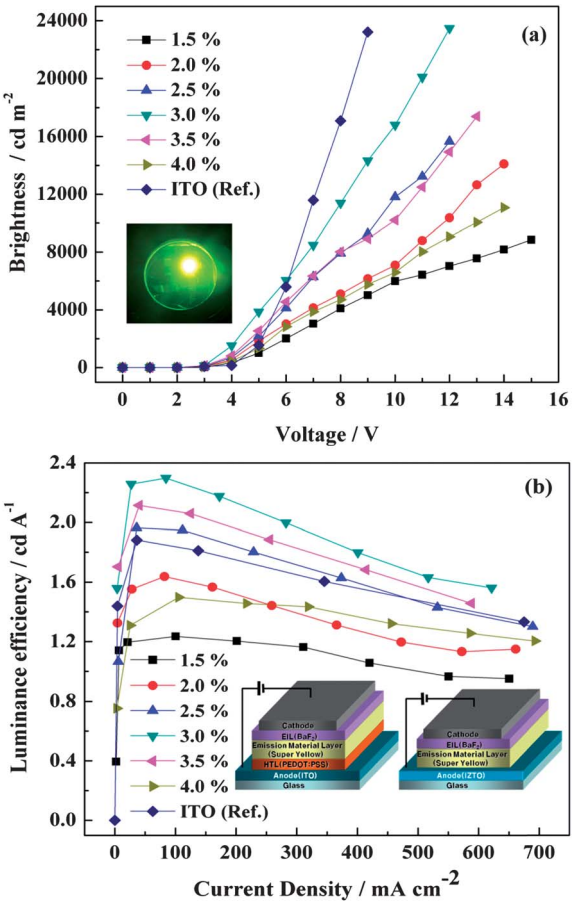

Fig. 10 (a) Brightness–voltage characteristics of PLEDs using IZTO films with various oxygen partial pressures and an ITO film as the reference (inset: luminescence image of PLEDs with an IZTO film), and (b) efficiency–current density characteristics of PLEDs using IZTO films with various oxygen partial pressures and an ITO film as the reference (inset: device structures of PLEDs).

Table 1 Characteristics of the IZTO film-based devices

Oxygen partial pressure [%]	Sheet resistance [Ω sq^{-1}]	Figure of merit [10^{-3} ohm^{-1}]	Turn on voltage [V]	Max. brightness [cd m^{-2}]	Max. efficiency [cd A^{-1}]	CIE coordinates	λ_{max} [nm]	Full width at half maximum [FWHM, nm]
1.5	70.9	0.4	3.0	8852	1.23	(0.46, 0.52)	542	92
2.0	59.1	1.5	2.8	14100	1.63	(0.44, 0.54)	542	84
2.5	42.5	2.1	2.8	15657	1.96	(0.43, 0.55)	542	78
3.0	35.8	3.0	2.8	23485	2.29	(0.42, 0.56)	542	75
3.5	67.1	2.3	2.8	17385	2.11	(0.41, 0.56)	542	70
4.0	90.2	1.4	2.7	11072	1.49	(0.40, 0.57)	542	66
[a]Reference	10	—	3.2	23228	1.88	(0.46, 0.52)	550	103

[a] ITO (170 nm)/PEDOT : PSS (40 nm)/Yellow polymer (80 nm)/BaF_2 (2 nm)/Ba (2 nm)/Al (200 nm).

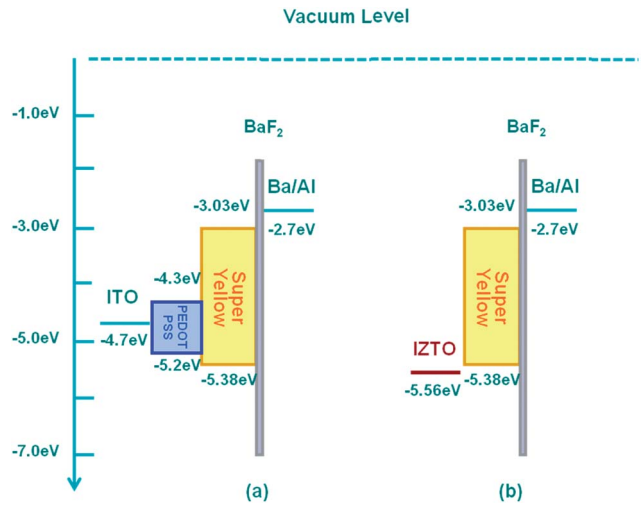

Fig. 11 Energy band diagrams of PLEDs with (a) ITO film and (b) IZTO film.

Fig. 12 shows the EL spectra of the PLEDs with IZTO anode films. The full width at half maximum (FWHM) of the EL spectra decreased with the increasing oxygen partial pressure. The FWHM at a 4.0% oxygen partial pressure was decreased by approximately 39% to 66 nm, compared with the value of 92 nm of the FWHM at a 1.5% oxygen partial pressure. This shows a better color purity result with a greater than 64% decrease of the FWHM of 103 nm of the PLEDs with the ITO film.

The device which applies a super yellow polymer as the emitting layer and uses the ITO film showed a maximum emission peak at 550 nm (λ_{max}) and CIE coordinates of (0.46, 0.52), as mentioned in Table 1. The λ_{max} value remained the same regardless of the oxygen partial pressure for the IZTO films, but there was a blue shift to 542 nm. The CIE coordinates remained the same as ITO (0.46, 0.52) at an oxygen partial pressure of 1.5% but the CIE coordinate shifted in the upper-left direction (0.40, 0.57) as the oxygen partial pressure was increased to 4.0%. This coordinate shift is due to the transmittance and absorbance change of the IZTO films. Fig. 6(a) shows that the IZTO film has the highest transmittance at wavelengths between 420 and 440 nm, depending on the oxygen partial pressures. On the other hand, the transmittance decreases between 420 and 490 nm. This means that the visible light within the wavelength region of 420 and 490 nm was absorbed. The λ_{max} value for the device with the ITO film was 550 nm, but it shifted to 542 nm due to visible light absorption within the wavelength region of 420 and 490 nm. The devices with the IZTO films have no shoulder peaks at 578 nm unlike the device with the ITO film, due to visible light absorption. Therefore, the FWHM of the EL spectra decreases with the increasing transmittance between 420 and 440 nm as the oxygen partial pressure in the IZTO films is increased, improving the color purity. Consequently, the FWHM of the EL spectra of the PLEDs with the IZTO films decreased by up to 64% compared to the PLEDs with the ITO film, which shows higher color purity.

Fig. 13 shows the results of the accelerated operation lifetime test of the devices. In the PLEDs with the ITO film, the extrapolated half-lifetime under a brightness of 15 000 cd m^{-2} was 21.5 h. However, the half-lifetime of the PLEDs with the IZTO film was 25.5 h, a 19% improvement, compared to the devices with ITO. In the case of the ITO/PEDOT : PSS structure, metal ions penetrate into the emitting layer after the ITO film is corroded by the strongly acidic PSS in PEDOT : PSS.[51,52] As a result, due to these metal ions in the emitting layer acting as quenching sites, the long-term stability was reduced. Therefore,

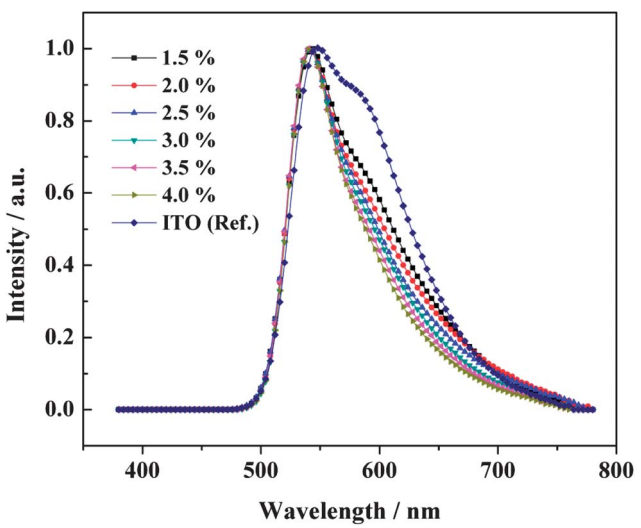

Fig. 12 EL spectra of PLEDs using IZTO films with various oxygen partial pressures, and using an ITO film.

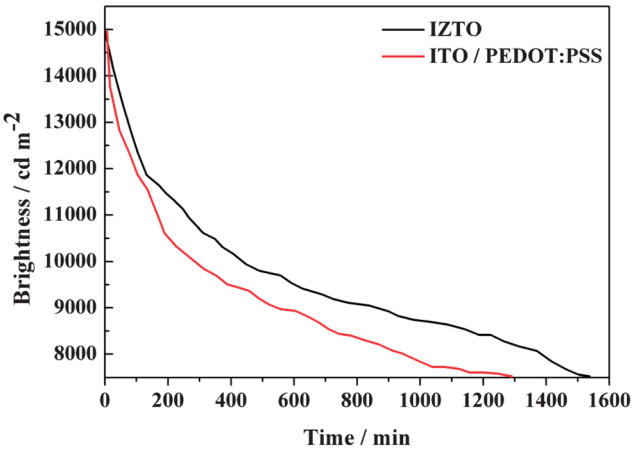

Fig. 13 Accelerated operation-lifetime tests of the IZTO and ITO devices.

it has been confirmed that the long-term stability was increased through the introduction of IZTO film to the PLEDs.

4 Conclusion

An IZTO target with over 20% less indium compared to the conventional ITO transparent conducting oxide was manufactured. The IZTO target is manufactured with the composition of In_2O_3 (70 at%)–ZnO (15 at%)–SnO_2 (15 at%). The IZTO films prepared at room temperature show a homogeneous and stable amorphous structure, a good smooth surface roughness of <0.5 nm, an optical energy band gap of >3.66 eV and a very high work function of >5.40 eV regardless of the oxygen partial pressure. The highest figure of merit (Φ_{TC}), of the IZTO film deposited at a 3% oxygen partial pressure, shows a maximum value of 3.0×10^{-3} ohm^{-1} as well as a transmittance of 81% (visible region), and the sheet resistance was 35.8 Ω sq^{-1}. In addition, the electrical properties, including the resistivity (ρ), mobility (μ) and carrier concentration (n), were 7.72×10^{-4} Ω cm, 44.59 cm^2 V s^{-1} and 1.92×10^{20} cm^{-3}, respectively.

The manufactured PLEDs showed the highest device performance with the IZTO film deposited at a 3% oxygen partial pressure, exhibiting a maximum brightness and maximum luminance efficiency of 23 485 cd cm^{-2} and 2.29 cd A^{-1}, respectively. This coincides with the figure of merit of the IZTO films, which showed a 21% enhancement in device performance compared to the PLEDs with the commercial ITO film. In addition, the FWHM of 75 nm of the EL spectra of the PLEDs with the IZTO films exhibited higher color purity, as evidenced by the reduction of 64% compared to the wide FWHM of 103 nm of the EL spectrum of the PLEDs with the ITO film. It was also confirmed that the PLEDs with the IZTO films were more stable than those with the ITO film. These results suggest that IZTO films are suitable for transparent electrodes in opto-electric applications.

Acknowledgements

This work was supported by the technology supporting project grant funded by the Korea Government Ministry of Knowledge Economy (no. 2012K10042360)

References

1 H. N. Wanka, M. B. Schubert and E. Lotter, *Sol. Energy Mater. Sol. Cells*, 1996, **41**, 519.
2 K. Imamori, A. Masuda and H. Matsumura, *Thin Solid Films*, 2001, **395**, 147.
3 H. Hosono, H. Ohta, M. K. Ueda and M. Hirano, *Vacuum*, 2002, **66**, 419.
4 L. J. Wang, S. Swensen, E. Polikarpov, D. W. Matson, C. C. Bonham, W. Bennett, D. J. Gaspar and A. B. Padmaperuma, *Org. Electron.*, 2010, **11**, 1555.
5 Y. F. Lan, W. C. Peng, Y. H. Lo and J. L. He, *Org. Electron.*, 2010, **11**, 670.
6 X. Xianwu, P. Zhiyong, D. Ying, Y. Lina and H. Shenghao, *Appl. Surf. Sci.*, 2007, **253**, 3345.
7 T. Minami, *Thin Solid Films*, 2008, **516**, 1314.
8 A. Subrahmanyam and U. K. Barik, *J. Phys. Chem. Solids*, 2005, **66**, 817.
9 G. J. Exarhos and X. D. Zhou, *Thin Solid Films*, 2007, **515**, 7025.
10 T. Minami, *MRS Bull.*, 2000, **25**, 38.
11 S. Sheng, G. J. Fang, C. Li, S. Xu and X. Z. Zhao, *Phys. Status Solidi A*, 2006, **203**, 1891.
12 J. Szczyrbowski, K. Schmalzbauer and H. Hoffmann, *Thin Solid Films*, 1986, **137**, 169.
13 K. L. Chopra, S. Major and D. K. Pandya, *Thin Solid Films*, 1983, **102**, 1.
14 Y. Shen, D. B. Jacobs, G. G. Malliaras, G. Koley, M. G. Spencer and A. Loannidis, *Adv. Mater.*, 2001, **13**, 1234.
15 D. R. Cairns, R. P. Witte, D. K. Sparacin, S. M. Sachsman, D. C. Paine, G. P. Crawford and R. R. Newton, *Appl. Phys. Lett.*, 2000, **76**, 1425.
16 K. A. Sierras, N. J. Morris, S. N. Kukureka and D. R. Cairns, *Wear*, 2009, **267**, 625.
17 K. A. Sierras, N. J.Morris, K. Ramji and D. R. Cairns, *Thin Solid Films*, 2009, **517**, 2590.
18 D. S. Hecht, L. Hu and G. Irvin, *Adv. Mater.*, 2011, **23**, 1482.
19 A. M. Alfantazi and R. R. Moskalyk, *Miner. Eng.*, 2003, **16**, 687.
20 M. A. Green, *Prog. Photovoltaics*, 2009, **17**, 347.
21 T. Minami, *Semicond. Sci. Technol.*, 2005, **20**, S35.
22 T. Minami, *Thin Solid Films*, 2008, **516**, 1314.
23 T. Minami, *Thin Solid Films*, 2008, **516**, 5822.
24 J. Cui, A. Wang, N. L. Edleman, J. Ni, P. Lee, N. R. Armstrong and T. J. Marks, *Adv. Mater.*, 2001, **13**(19), 1476.
25 W. H. Baek, M. Choi, T. S. Yoon, H. H. Lee and Y. S. Kim, *Appl. Phys. Lett.*, 2010, **96**, 133506.
26 L. M. Wong, S. Y. Chiam, J. Q. Huang, S. J. Wang, J. S. Pan and W. K. Chim, *Appl. Phys. Lett.*, 2011, **98**, 022106.
27 B. S. Chun, H. C. Wu, M. Abid, I. C. Chu, S. Serrano-Guisan, I. Shvets, V. Daniel and S. Choi, *Appl. Phys. Lett.*, 2010, **97**, 082109.
28 J. M. Phillips, R. J. Cava, G. A. Thomas, S. A. Carter, J. Kwo, T. Siegrist, J. J. Krajewski, J. H. Marshall, W. F. Peck, Jr and D. H. Rapkine, *Appl. Phys. Lett.*, 1995, **67**, 2246.
29 T. Minami, T. Yamamoto, Y. Toda and T. Miyata, *Thin Solid Films*, 2000, **373**, 189.

30 C. A. Hoel, T. O. Mason, J. F. Caillard and K. R. Poeppelmeier, *Chem. Mater.*, 2010, **22**, 3569.
31 J.-H. Bae, J.-M. Moon, S. W. Jeong, J.-J. Kim, J.-W. Kang, D.-G. Kim, J.-K. Kim, J.-W. Park and H.-K. Kim, *J. Electrochem. Soc.*, 2008, **155**, J1.
32 G.-S. Heo, Y. Matsumoto, I.-G. Gim, H.-K. Lee, J.-W. Park and T.-W. Kim, *Solid State Commun.*, 2010, **150**, 223.
33 Y. D. Ko, C. H. Lee, D. K. Moon and Y. S. Kim, *Thin Solid Flims*, 2013, DOI: 10.1016/j/tsf.2013.05.069.
34 B. Yaglioglu, H. Y. Yeom and D. C. Paine, *Appl. Phys. Lett.*, 2006, **89**, 062103.
35 R. Tahar, T. Ban, Y. Ohya and Y. Takahashi, *J. Appl. Phys.*, 1998, **83**, 2631.
36 L. S. Hung and C. H. Chen, *Mater. Sci. Eng., R*, 2002, **39**, 143.
37 C. W. Wo-Yang, H. Yeom and D. C. Paine, *Thin Solid Films*, 2008, **516**, 3105.
38 J. Meng, J. Gao, R. A. Silva and S. Song, *Thin Solid Films*, 2008, **516**, 5454.
39 N. Naghavi, C. Marcel, L. Dupont, A. Rougier, J.-B. Leriche and C. Guery, *J. Mater. Chem.*, 2000, **10**, 2315.
40 J. R. Bellingham, W. A. Phillips and C. J. Adkins, *J. Phys.: Condens. Matter*, 1990, **2**, 6207.
41 C. W. W. Yang, H. Yeom and D. C. Paine, *Thin Solid Films*, 2008, **516**, 3105.
42 D. Y. Lee, J. R. Lee, G. H. Lee and P. K. Song, *Surf. Coat. Technol.*, 2008, **202**, 5718.
43 L. J. Meng, J. Gao, R. A. Silva and S. Song, *Thin Solid Films*, 2008, **516**, 5454.
44 S. T. Tan, B. J. Chen, X. W. Sun, W. J. Fan, H. S. Kwok, X. H. Zhang and S. J. Chua, *J. Appl. Phys.*, 2005, **98**, 013505.
45 E. Burstein, *Phys. Rev.*, 1954, **93**, 632.
46 G. Sanon, R. Rup and A. Mansingh, *Phys. Rev. B: Condens. Matter Mater. Phys.*, 1991, **44**, 5672.
47 H. Han, J. W. Mayer and T. L. Alford, *J. Appl. Phys.*, 2006, **100**, 083715.
48 J. C. C. Fan and J. B. J. Goodenough, *J. Appl. Phys.*, 1977, **48**, 3524.
49 K. Sugiyama, H. Ishii, Y. Ouchi and K. Seki, *J. Appl. Phys.*, 2000, **87**, 295.
50 G. J. Haacke, *J. Appl. Phys.*, 1976, **47**, 4086.
51 I. S. Song, S. W. Heo, J. R. Ku and D. K. Moon, *Thin Solid Films*, 2012, **520**, 4068.
52 S. W. Heo, E. J. Lee, K. W. Seong and D. K. Moon, *Sol. Energy Mater. Sol. Cells*, 2013, **115**, 123.